Cell

C. elegans Screen Identifies Autophagy Genes Specific to Multicellular Organisms

Ye Tian,[1,2,5] Zhipeng Li,[1,5] Wanqiu Hu,[3,5] Haiyan Ren,[1,5] E. Tian,[1] Yu Zhao,[1] Qun Lu,[1] Xinxin Huang,[1] Peiguo Yang,[1] Xin Li,[1] Xiaochen Wang,[1] Attila L. Kovács,[4] Li Yu,[3,*] and Hong Zhang[1,*]

[1]National Institute of Biological Sciences, Beijing 102206, P.R. China
[2]College of Life Sciences, Beijing Normal University, Beijing 100875, P.R. China
[3]State Key Laboratory of Biomembrane and Membrane Biotechnology, School of Life Sciences, Tsinghua University, Beijing 100084, P.R. China
[4]Department of Anatomy, Cell and Developmental Biology, Eötvös Loránd University, Budapest 1117, Hungary
[5]These authors contributed equally to this work
*Correspondence: liyulab@mail.tsinghua.edu.cn (L.Y.), zhanghong@nibs.ac.cn (H.Z.)
DOI 10.1016/j.cell.2010.04.034

SUMMARY

The molecular understanding of autophagy has originated almost exclusively from yeast genetic studies. Little is known about essential autophagy components specific to higher eukaryotes. Here we perform genetic screens in *C. elegans* and identify four metazoan-specific autophagy genes, named *epg-2*, *-3*, *-4*, and *-5*. Genetic analysis reveals that *epg-2*, *-3*, *-4*, and *-5* define discrete genetic steps of the autophagy pathway. *epg-2* encodes a coiled-coil protein that functions in specific autophagic cargo recognition. Mammalian homologs of EPG-3/VMP1, EPG-4/EI24, and EPG-5/mEPG5 are essential for starvation-induced autophagy. VMP1 regulates autophagosome formation by controlling the duration of omegasomes. EI24 and mEPG5 are required for formation of degradative autolysosomes. This study establishes *C. elegans* as a multicellular genetic model to delineate the autophagy pathway and provides mechanistic insights into the metazoan-specific autophagic process.

INTRODUCTION

Autophagy, an evolutionarily conserved intracellular catabolic process, involves formation of a double-membrane structure, called the autophagosome, which engulfs portions of the cytosol and delivers them to lysosomes for degradation (Xie and Klionsky, 2007; Mizushima, 2007; Nakatogawa et al., 2009). In higher eukaryotes, autophagy is important for diverse processes, such as adaptation to starvation and stress, removal of aggregate-prone proteins, and elimination of pathogens (Mizushima, 2007; Meléndez and Neufeld, 2008). Deregulated autophagy has been linked to pathologic conditions such as neurodegeneration, cardiomyopathy, and tumor progression (Levine and Kroemer, 2008).

The autophagy pathway has several distinct steps: initial formation of a cup-shaped membrane sac, called the isolation membrane or phagophore (autophagosome nucleation step), expansion and closure of the double-membrane structure (autophagosome expansion and completion step), fusion of the autophagosome to the lysosome, and degradation of cargo inside the autolysosome (Xie and Klionsky, 2007; Nakatogawa et al., 2009). In yeast, about 20 *ATGs* (autophagy-related genes) are essential for both starvation-induced autophagy and the autophagy-related Cvt pathway. Autophagosome nucleation requires the Atg1/Atg13 protein kinase complex and the Atg6/Vps34 class III phosphatidylinositol 3-kinase (PI(3)K) complex; expansion and completion of the autophagosome is regulated by the two ubiquitin-like conjugation systems, which consist of ubiquitin-like proteins (Atg8 and Atg12), an E1-like activating enzyme (Atg7), and E2-like conjugating enzymes (Atg3 and Atg10). Atg12 forms a conjugate with Atg5, whereas Atg8 is conjugated to phosphatidylethanolamine (PE) (Xie and Klionsky, 2007; Nakatogawa et al., 2009). Almost all known Atg proteins at least transiently associate with and act in a hierarchical order in organizing the pre-autophagosomal structure (PAS), which is thought to be the site for autophagosome assembly in yeast (Suzuki et al., 2007). However, the molecular mechanism by which Atg proteins collaborate to form autophagosomes is largely unknown.

Studies of autophagy in higher eukaryotes are greatly facilitated by the functional conservation of yeast Atg proteins (Mizushima, 2007). However, autophagy in higher eukaryotes involves much more complex membrane dynamics. Mammalian cells have no defined PAS and several isolation membranes can form simultaneously from multiple sites in the cytoplasm (Mizushima, 2007). At least some autophagosomes originate from omegasomes, which are phosphatidylinositol 3-phosphate (PI(3)P)-enriched subdomains of the endoplasmic reticulum (ER) (Axe et al., 2008; Hayashi-Nishino et al., 2009). In higher eukaryotes, nascent autophagosomes undergo stepwise maturation and autophagosomes fuse with large numbers of lysosomes (Eskelinen, 2005; Fader and Colombo, 2008; Longatti and Tooze, 2009), whereas in yeast no maturation step has been reported and autophagosomes directly fuse with the single large acidic vacuole. Finally, lysosome components are retrieved from autolysosomes after cargo degradation, a process called autolysosome reformation (Yu et al., 2010). Thus, it is conceivable that

the higher eukaryote autophagy pathway might require more elaborate molecular machinery, including factors that are absent in yeast. So far, very little is known about higher eukaryote-specific autophagy components.

We showed previously that autophagy is required for degradation of germline P granule components, PGL-1 and PGL-3, in somatic cells during *C. elegans* embryogenesis, resulting in their exclusive distribution in germline precursor cells (Zhang et al., 2009). Loss of autophagy activity causes PGL-1 and PGL-3 to accumulate into aggregates, termed PGL granules, in somatic cells. Formation and autophagic degradation of PGL granules requires zygotically synthesized SEPA-1 that colocalizes with PGL aggregates in autophagy mutants (Zhang et al., 2009). SEPA-1 itself forms aggregates and is also preferentially removed by autophagy during embryogenesis, resulting in SEPA-1 aggregates present only in early embryos (Zhang et al., 2009). Here we performed genetic screens to isolate mutants with defective degradation of autophagy substrates and identified four previously uncharacterized, higher eukaryote-specific autophagy genes, *epg-2*, *-3*, *-4*, and *-5*, which define discrete genetic steps in the autophagy pathway. The mammalian EPG-3, -4, and -5 homologs are essential for starvation-induced autophagy. Knockdown of *VMP1* extends the duration of omegasomes and consequently causes a defect in autophagosome formation. Reduced levels of EI24 and mEPG5 result in accumulation of degradation-defective autolysosomes. Our study establishes *C. elegans* as a multicellular genetic model to delineate the autophagy pathway.

RESULTS

Genetic Screens for Mutants with Defective Autophagic Degradation of PGL Granules and the *C. elegans* p62 Homolog

PGL granule components and the *C. elegans* p62 homolog, T12G3.1, are selectively removed by autophagy during embyogenesis (Figures 1A, 1B, 1G, and 1H; Figure S1 available online). We performed genetic screens to identify mutants with defective degradation of GFP::PGL-1, SEPA-1::GFP, or T12G3.1::GFP in somatic cells during embryonic stages. From ~30,000 genomes screened, we obtained ~160 mutants. These included mutations in yeast *ATG* gene homologs, including *atg-2, -3*, *-4*, *-5, -7*, *-9, -10*, *-13*, *-16, -18*, and *lgg-1* (the *C. elegans* ATG8 homolog) (Figure 1M). We also identified four genes, named *epg-2, -3*, *-4*, and *-5* (ectopic *P*GL *g*ranules), that did not map to known *Atg* loci.

In *epg-2, -3*, *-4*, and *-5* mutants, somatic GFP::PGL-1-positive granules formed in embryos and large numbers of SEPA-1 aggregates persisted in late-stage embryos and early larvae (Figures 1C–1F; Figure S1). In addition to the GFP reporters, endogenous PGL granule components PGL-1, PGL-3, and SEPA-1 also formed many aggregates and were colocalized in *epg-2, -3*, *-4*, and *-5* mutants (Figure S1 and data not shown). Endogenous PGL-3 protein levels remained high in late-stage *epg-2, -3*, *-4*, and *-5* mutant embryos (Figure S1), whereas *pgl-3* mRNA levels were unchanged (data not shown).

In wild-type embryos, T12G3.1, shown by the GFP reporter or anti-T12G3.1 antibody, was very weakly expressed and diffusely localized in the cytoplasm (Figures 1G and 1H; Figure S1). In known autophagy mutants and *epg-3*, *-4*, and *-5* mutants, embryonic expression of T12G3.1 greatly increased and formed large numbers of aggregates (Figures 1J–1L; Figure S1). *t12 g3.1* mRNA levels were unchanged in *epg-3*, *-4*, and *-5* mutants (data not shown). C35E7.6 and ZK1053.4, two other preferential embryonic autophagy targets from the SEPA-1 family (Zhang et al., 2009), also ectopically accumulated in *epg-3*, *-4*, and *-5* mutants (Figure S1). *epg-3*, *-4*, and *-5* mutations also caused other defects associated with loss of autophagy, such as reduced survival of newly hatched L1 larvae in the absence of food (Figure S1). Mutations in *epg-2*, however, did not affect the expression of T12G3.1, C35E7.6, and ZK1053.4 (Figure 1I; Figure S1). Therefore, *epg-3*, *-4*, and *-5* are involved in degrading various autophagy substrates, whereas *epg-2* appears to be specifically involved in degradation of PGL granules.

epg-2 Encodes a Nematode-Specific Protein, and *epg-3, -4*, and *-5* Encode Proteins with Homologs in Mammals

epg-2, -3, -4, and *-5* were genetically mapped and cloned by transformation rescue. A transgene carrying a single gene, Y39G10AR.10, rescued the defective degradation of somatic PGL granules in *epg-2* mutants (Figure S2). *epg-2* encodes a 690 amino acid protein with multiple coiled-coil domains (Figure S2). Glutamines at codons 122 and 489 were mutated to stop codons in *bp287* and *bp444* mutants, respectively (Figure S2). EPG-2 appears to be specific to nematodes. However, coiled-coil domains may not be conserved at the level of primary sequence, so the functional EPG-2 homolog may still exist in other organisms.

The PGL granule degradation defect in *epg-3* mutants was rescued by a transgenic array containing a single gene Y37D8A.22, which encodes a 458 amino acid protein (Figure S2). Molecular lesions were identified in *epg-3(bp424*, *bp405*, or *bp677)* mutants. EPG-3 has 48% identity and 69% similarity (Blast e value: $4e^{-111}$) with human VMP1 (vacuolar membrane protein 1), which is highly expressed in a pancreas with acute pancreatitis (Dusetti et al., 2002). Amazingly, human *VMP1* rescued the somatic PGL granule degradation defect in *epg-3* mutants (Figure S3), indicating functional conservation. EPG-3 is highly conserved in *Arabidopsis*, *Drosophila*, and mammals, but no homolog is present in *S. cerevisiae*.

The rescuing activity for *epg-4* was mapped to F37C12.2, which encodes a protein of 315 amino acids (Figure S2). In *bp425* and *bp623* mutants, the consensus nucleotide G of the 3′ splice site was mutated to A in the second and third introns of *epg-4*, respectively. EPG-4 has 28% identity and 47% similarity (Blast e value: $1e^{-29}$) with human EI24/PIG8 (etoposide-induced gene 24 and p53-induced gene 8), expression of which is strongly activated by the tumor suppressor protein p53 and by etoposide, a genotoxic agent that activates p53 (Gu et al., 2000). Both EPG-4 and EI24/PIG8 possess six transmembrane domains (Figure S2). EPG-4 has homologs in *Arabidopsis*, *Drosophila*, and mammals, but not *S. cerevisiae*.

epg-5 rescuing activity localized to a single gene C56C10.12, which encodes a 1599 amino acid protein (Figure S2). Molecular lesions were identified in *epg-5* mutants. EPG-5 has 21% identity and 41% similarity (Blast e value: $1e^{-57}$) to human KIAA1632 (here named mEPG5), which was identified as a candidate breast cancer gene in a systematic analysis of genetic alterations

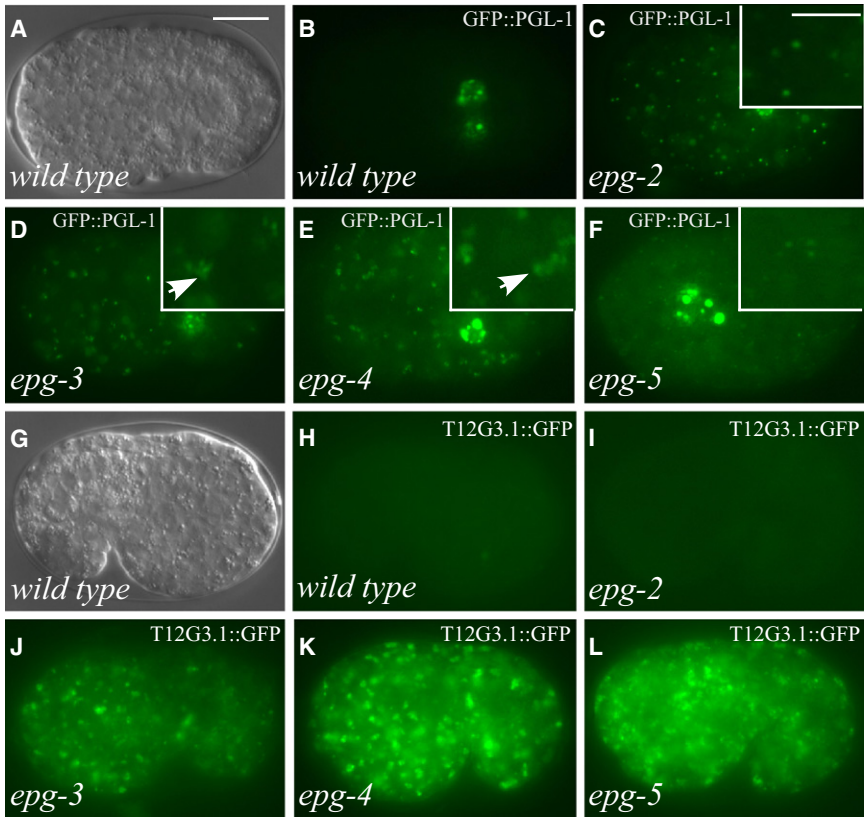

Figure 1. Mutations in *epg-2, -3, -4*, and *-5* Cause Defective Degradation of PGL Granules and the *C. elegans* p62 Homolog

Scale bars (10 μm for whole embryos, 5 μm for inserts) are only shown once in each figure because *C. elegans* embryos remain the same size during embryogenesis.

(A–F) GFP::PGL-1-labeled P granules are restricted to germ precursor cells in a wild-type embryo (A and B) but ectopically accumulate in somatic cells in *epg-2*, *-3*, *-4*, and *-5* mutant embryos. Arrows show PGL granule clusters.

(G–L) The *C. elegans* p62 homolog, T12G3.1, is weakly expressed in wild-type and *epg-2* embryos but forms large numbers of aggregates in *epg-3*, *-4*, and *-5* mutant embryos. (A and G) Nomarski images of the embryos in (B) and (H).

(M) Summary of autophagy mutants identified in the genetic screen.

See also Figure S1.

M

yeast Atg gene	*C. elegans* ATG homolog	number of alleles identified	metazoan specific gene	number of alleles identified
atg-2	*atg-2*	4	*epg-2*	3
atg-3	*atg-3*	12	*epg-3/VMP1*	3
atg-4	*atg-4.1*	11	*epg-4/EI24*	2
atg-5	*atg-5*	2	*epg-5/mEPG5*	16
atg-7	*atg-7*	14	*epg-7/FIP200*	7
atg-8	*atg-8/lgg-1*	4		
atg-9	*atg-9*	18		
atg-10	*atg-10*	2		
atg-13	*atg-13/epg-1*	2		
atg-16	*atg-16.2*	2		
atg-18	*atg-18*	3		

in breast tumors (Sjöblom et al., 2006). EPG-5 is highly conserved in *Drosophila* and mammals, but no homolog was identified in *Dictyostelium*, *Arabidopsis*, and *S. cerevisiae*.

epg-2, -3, -4, and *-5* Are Widely Expressed

Antibody staining revealed that EPG-2 was diffusely localized in the cytoplasm and formed aggregates at early embryonic stages (Figure 2A). EPG-2 aggregates peaked in abundance at the ~100 cell stage, then decreased, becoming almost undetectable at the comma stage (Figures 2B and 2C). Diffuse EPG-2 persisted in late-stage embryos (data not shown). A functional *gfp::epg-2* reporter had the same expression pattern as endogenous *epg-2* (data not shown).

Functional translational fusion reporters showed that *epg-3*, *-4*, and *-5* were ubiquitously expressed during embryogenesis (Figure 2). At post-embryonic stages, *epg-3*, *-4*, and *-5* were widely expressed, including in pharyngeal and body wall muscles and intestine cells (Figures 2F, 2I, and 2O). EPG-3::GFP and EPG-5::GFP were diffusely localized in the cytoplasm. EPG-4::GFP formed a diffuse reticular network throughout the cytoplasm and also accumulated into a ring structure surrounding the nucleus, reminiscent of ER localization (Figures 2H and 2I). EPG-4::GFP colocalized with the ER-specific marker cherry::TRAM-1, confirming that EPG-4 is an ER-localized protein (Figures 2J–2L).

epg-3 and *epg-4* Mutants Exhibit Distinct Distribution and Organization of PGL Granules

PGL granules were spherical and evenly dispersed in the cytoplasm at all embryonic stages in *lgg-1* and *atg-3* mutants (Figure 3A). However, in *epg-3* and *epg-4* mutants, PGL granules formed clusters from the ~100 cell stage onward (Figures 3B and 3C). Within a cluster, PGL granules formed enlarged tubular structures or giant complexes consisting of several interconnected aggregates (Figures 3B and 3C). T12G3.1 also formed clusters and exhibited the same distribution pattern as PGL granules in *epg-3* and *epg-4* mutants (Figure S4). In *atg-3* and *lgg-1* mutants, T12G3.1 aggregates were in close proximity to but separate from PGL granules, whereas in *epg-3* and *epg-4* mutants, the fluorescent signals from PGL granules and T12G3.1 aggregates partially overlapped (Figure S4). Thus, the organization of PGL granules and T12G3.1 aggregates in *epg-3* and *epg-4* mutants is distinct from that in *lgg-1* and *atg-3* mutants.

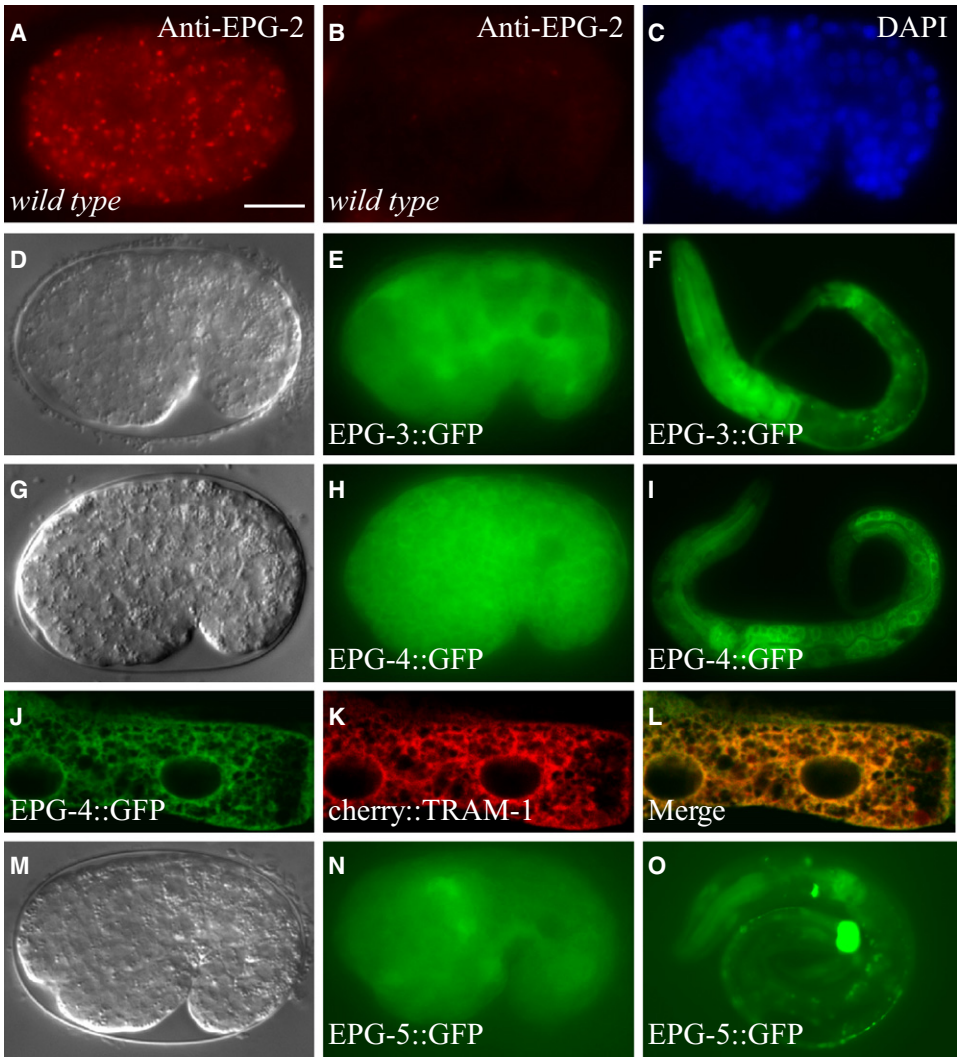

Figure 2. *epg-2*, *-3*, *-4*, and *-5* Are Widely Expressed

(A–C) EPG-2 aggregates, detected by anti-EPG-2 antibody, are seen in an ~100 cell stage embryo (A) but are absent in a comma stage embryo (B). (C): DAPI image of the embryo in (B).

(D–O) Reporters for *epg-3*, *-4*, and *-5* are expressed ubiquitously in embryos (E, H, and N) and widely in larvae (F, I, and O). EPG-3 and EPG-5 are cytoplasmic. EPG-4::GFP colocalizes with the ER marker cherry::TRAM-1 (J–L). (D, G, and M) Nomarski images of the embryos in (E), (H), and (N).

See also Figure S2 and Figure S3.

LGG-1-Labeled Autophagic Structures Are Enlarged in *epg-3* and *epg-4* Mutants

We next investigated autophagosome biogenesis during embryogenesis in *epg-3* and *epg-4* mutants by monitoring the localization of LGG-1/Atg8, which associates with autophagic membranes (Mizushima et al., 2010). The anti-LGG-1 antibody detected two forms of LGG-1, namely LGG-1-I and LGG-1-II (probably the lipid-conjugated form of LGG-1) (Figure 3F). In wild-type embryos, in addition to diffuse cytoplasmic localization, LGG-1 also formed aggregates that mostly appeared at the ~100 to 200 cell stage and persisted throughout embryogenesis (Figure 3G; Figure S5). In *atg-3* and *atg-7* mutants, LGG-1-II- and LGG-1-positive puncta could not be detected (Figures 3F and 3H and data not shown), consistent with the notion that *atg-3* and *atg-7* are required for lipid conjugation of LGG-1 and that only the lipid-conjugated form of LGG-1 accumulates on autophagic structures. In *epg-3* and *epg-4* mutants, both forms of LGG-1 accumulated and LGG-1 puncta were formed at all stages of embryogenesis and were bigger in size and stronger in intensity (Figures 3F, 3I, and 3J). Like PGL granules and T12G3.1 clusters, LGG-1 puncta in *epg-3* and *epg-4* mutants were irregular in shape, forming enlarged tubular structures and giant complexes with punctate interconnections (Figures 3M and 3N).

To determine at which step degradation of PGL granules is defective in *epg-3* and *epg-4* mutants, we examined the distribution of SEPA-1 aggregates and LGG-1 puncta. In wild-type ~200 cell stage embryos, ~67% of SEPA-1 aggregates colocalized with LGG-1 puncta, whereas the rest were located

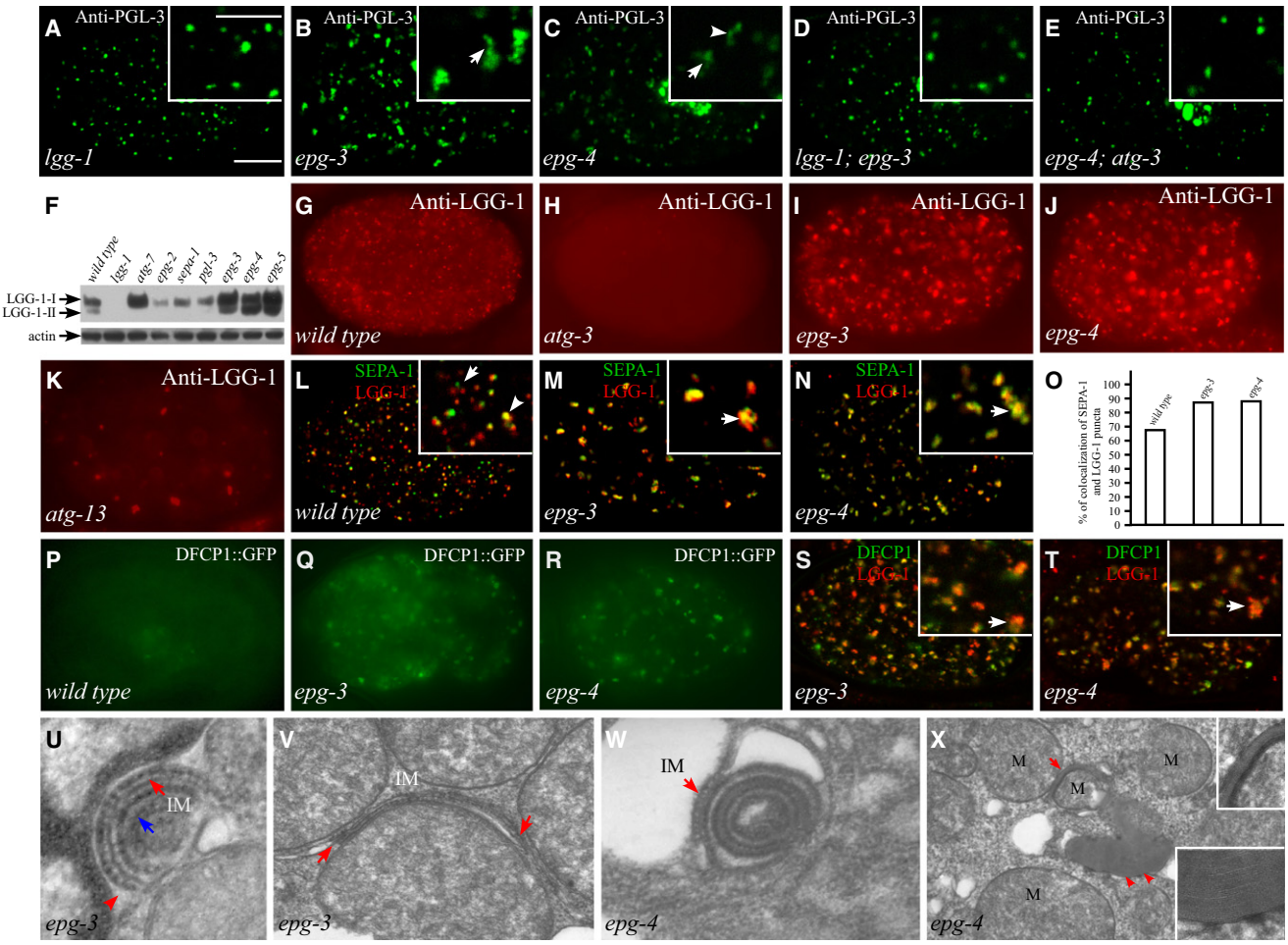

Figure 3. *epg-3* and *epg-4* Regulate an Early Step of Autophagosome Formation

(A) PGL granules are evenly dispersed in *lgg-1* mutants.

(B and C) PGL granules form clusters (arrows in the inserts) in *epg-3* and *epg-4* mutant embryos. The arrowhead indicates a tubular structure.

(D and E) PGL granules are dispersed in *lgg-1; epg-3* and *epg-4; atg-3* double mutant embryos.

(F) Western analysis showing two forms of LGG-1 in wild-type animals. Levels of LGG-1-I and LGG-1-II are increased in *epg-3*, *-4*, and *-5* mutants.

(G) LGG-1 forms puncta in wild-type embryos.

(H) No LGG-1 puncta are detected in *atg-3* mutant embryos.

(I–K) LGG-1 forms large punctate structures in *epg-3* (I) and *epg-4* (J) mutants and also in a few cells in *atg-13* mutants (K).

(L) In a wild-type embryo, SEPA-1 aggregates colocalize with (arrowhead in the insert), or locate close to (arrow in the insert), LGG-1 puncta.

(M and N) SEPA-1 aggregates colocalize with LGG-1 puncta in *epg-3* (M) and *epg-4* (N) mutant embryos at the ~100 to ~200 cell stage (arrows in the inserts).

(O) Percentage of SEPA-1 aggregates colocalizing with LGG-1 puncta. Wild-type: 66.7% (n = 435); *epg-3*: 86.4% (n = 250), *epg-4*: 87.8% (n = 278). n: number of SEPA-1 aggregates examined.

(P) In a wild-type comma stage embryo, weak DFCP1::GFP signal is diffusely localized.

(Q and R) DFCP1::GFP forms punctate structures in *epg-3* (Q) and *epg-4* (R) mutant comma stage embryos.

(S and T) DFCP1::GFP-labeled punctate structures colocalize with LGG-1 puncta (arrows in the inserts) in *epg-3* (S) and *epg-4* (T) mutant embryos. Separate images are shown in Figure S6.

(U) An isolation membrane (IM) (red arrow) is found surrounding RER cisterns (arrowhead: outer RER; blue arrow: inner RER) in an *epg-3* mutant.

(V) An isolation membrane is found between mitochondria in an *epg-3* mutant.

(W) An isolation membrane structure (arrow) is found around RER cisterns in an *epg-4* mutant.

(X) Possible IM-related membrane structures in *epg-4* mutants. The arrow indicates a multilayered membrane structure between and around mitochondria (M) (enlarged, top right). Arrowheads indicate an expanded multilayered membrane stack (enlarged, lower right).

See also Table S1, Figure S4, Figure S5, and Figure S6.

close to LGG-1 puncta (Figures 3L and 3O). LGG-1 puncta in *epg-3* and *epg-4* mutants were almost completely colocalized with PGL granules (Figures 3M–3O; Figure S5). These results suggest that in *epg-3* and *epg-4* mutants the PGL granules are enwrapped or surrounded by the LGG-1-labeled autophagic structures.

Omegasomes and Isolation Membranes Accumulate in *epg-3* and *epg-4* Mutants

Omegasomes, which are transient PI(3)P-enriched ER subdomains that can be specifically labeled by DFCP1, form a cradle for autophagosome formation (Axe et al., 2008). In wild-type animals, DFCP1::GFP formed punctate structures in pharyngeal muscles and several other tissues with autophagy activity (Figure S6) (Kovács and Zhang, 2010). Weak diffuse DFCP1::GFP signal, but not punctate structures, was detected in the cytoplasm at all embryonic stages (Figure 3P; Figure S6), suggesting that omegasomes are transient during embryonic development. However, in *epg-3* and *epg-4* mutant embryos there was a dramatic accumulation of DFCP1::GFP punctate structures that colocalized with LGG-1 puncta (Figures 3Q–3T; Figure S6). These results suggest that omegasomes accumulate in *epg-3* and *epg-4* mutant embryos and the accumulated LGG-1 puncta are probably early autophagic structures such as isolation membranes.

We next examined the autophagic structures in *epg-3* and *-4* mutants by transmission electron microscopy (TEM). Typical autophagic structures could not be observed by EM in early *C. elegans* embryos, probably due to their low number (estimated from the number of LGG-1 puncta per cell), rapid cell division, and fast autophagic process (Sigmond et al., 2008). Autophagic structures could be detected in larvae and adults. The earliest autophagic structure detectable by EM is the isolation membrane, which appears as two thin ribosome-free membranes typically having an empty cleft between them or being closely apposed to each other (in some places pentalaminar) (Sigmond et al., 2008). Isolation membranes are very rarely observed in wild-type *C. elegans*; indeed, we observed only two in >5000 images from several hundred animals. However, in *epg-3* and *epg-4* mutants, isolation membranes were readily detected surrounding the rough endoplasmic reticulum (RER) or the mitochondrion, which are two possible sources of autophagosomal membranes (Figures 3U–3W; Figure S6). The number of isolation membranes is at least two orders of magnitude higher than in wild-type animals. For example, we found 2, 2, and 3 isolation membrane profiles in cytoplasmic areas of 16, 68, and 51 μm^2, respectively, in three late *epg-3* larvae. Isolation membranes in *epg-3* and *epg-4* mutants were also much larger than the rare ones seen in wild-type animals. In *epg-4* mutants, there were also structures with multiple membrane layers that surrounded cytoplasmic areas (Figure 3X). Furthermore, *epg-4* mutants had a large number of ribosome-free double-membrane structures with wide clefts between the two membrane sheets, which in some cases seemed to be continuous with the RER (Figure S6), suggesting that the flow of membrane material toward the isolation membrane might be inhibited. These data indicate that the formation and closure of isolation membranes are severely retarded in *epg-3* and *epg-4* mutants.

Genetic Interactions between *epg-3*, *epg-4*, and Other Known Autophagy Mutants

To investigate the genetic interactions between *epg-3* and *epg-4* and other known *atg* genes, we examined the distribution and organization of PGL granules and LGG-1 puncta. As in *atg-3* and *lgg-1* mutants, PGL granules were spherical and dispersed and no LGG-1 puncta were formed in *atg-5* and *atg-10* mutants (Table S1). *epg-3* and *epg-4* mutants in combination with a mutation in *atg-3*, *lgg-1*, or *atg-10* displayed the same distribution and organization of PGL granules as *atg-3*, *lgg-1*, and *atg-10* single mutants and, as expected, no LGG-1 puncta were formed in the double mutants (Figures 3D and 3E; Figure S4; Table S1).

In mutants for *unc-51* (encoding the *C. elegans* Atg1 homolog) and *atg-13/epg-1*, the size and organization of PGL granules were indistinguishable from those in mutants of the two ubiquitin-like conjugation systems (Figure S5; Table S1). LGG-1 puncta were absent from most embryonic cells in *unc-51* and *atg-13* mutants, but in a few cells they accumulated into large aggregates (Figure 3K; Figure S5). Loss of function of *unc-51* or *atg-13* completely suppressed the phenotype of the formation and distribution of PGL granules and LGG-1 puncta in *epg-3* and *epg-4* mutants (Table S1).

In yeast, Atg18 interacts with Atg2 and is recruited to autophagic membranes by binding of Atg18 to PI(3)P (Nakatogawa et al., 2009). In *atg-18* mutants, PGL granules formed widely dispersed spherical structures, and LGG-1 formed puncta that did not colocalize with PGL granules (Figure S5; Table S1). The PGL granule/LGG-1 puncta phenotype in *epg-3; atg-18* and *epg-4; atg-18* mutants resembled that in *epg-3* and *epg-4* single mutants (Table S1). Surprisingly, we found that the *atg-2* mutant phenotype was similar to *epg-3* and *epg-4* mutants; PGL granules and T12G3.1 aggregates formed clusters and LGG-1 puncta were also enlarged and colocalized with PGL aggregates in *atg-2* mutants (Figure S5), indicating that *atg-2* and *atg-18* have distinct functions in the autophagy pathway.

The *epg-3*, *epg-4*, *lgg-1*, *unc-51, atg-13*, and *atg-18* mutant alleles used in the epistasis analysis are putative null. The genetic interactions suggest that *epg-3* and *epg-4* are likely to act downstream of the Atg1/Atg13 complex but upstream of *atg-18* in the autophagic degradation of protein aggregates. As expected, the two ubiquitin-like conjugation systems are required for the formation of LGG-1 puncta in *epg-3* and *epg-4* mutants.

epg-5 Functions at a Step Distinct from *epg-3*, *epg-4*, and Other Autophagy Genes

In *epg-5* mutants, PGL granules and T12G3.1 aggregates were spherical and widely dispersed in the cytoplasm, and most PGL granules and T12G3.1 aggregates were in close proximity but did not colocalize (Figures 4A and 4D; Figure S4). However, compared to *atg-3* and *lgg-1* mutants, there were more PGL granules and T12G3.1 aggregates and their size was smaller (Figure 4A). Compared to wild-type, both forms of LGG-1 accumulated in *epg-5* mutant embryos and there were more LGG-1 puncta, which resembled PGL granules in size and shape (Figure 4G; Figure S5). SEPA-1 aggregates still colocalized with LGG-1 puncta in *epg-5* mutants, and the level of colocalization increased as development proceeded (Figures 4J and 4L and data not shown).

We investigated the genetic interactions between *epg-5* and other autophagy mutants. The small size and increased number of PGL granules and colocalization of PGL granules and LGG-1 puncta in *epg-5* null mutants were suppressed by loss of function of *atg-3*, *atg-13*, and *atg-5* (Figures 4B, 4E, and 4H; Figure S4; Table S1). Simultaneous depletion of *epg-3, epg-4*,

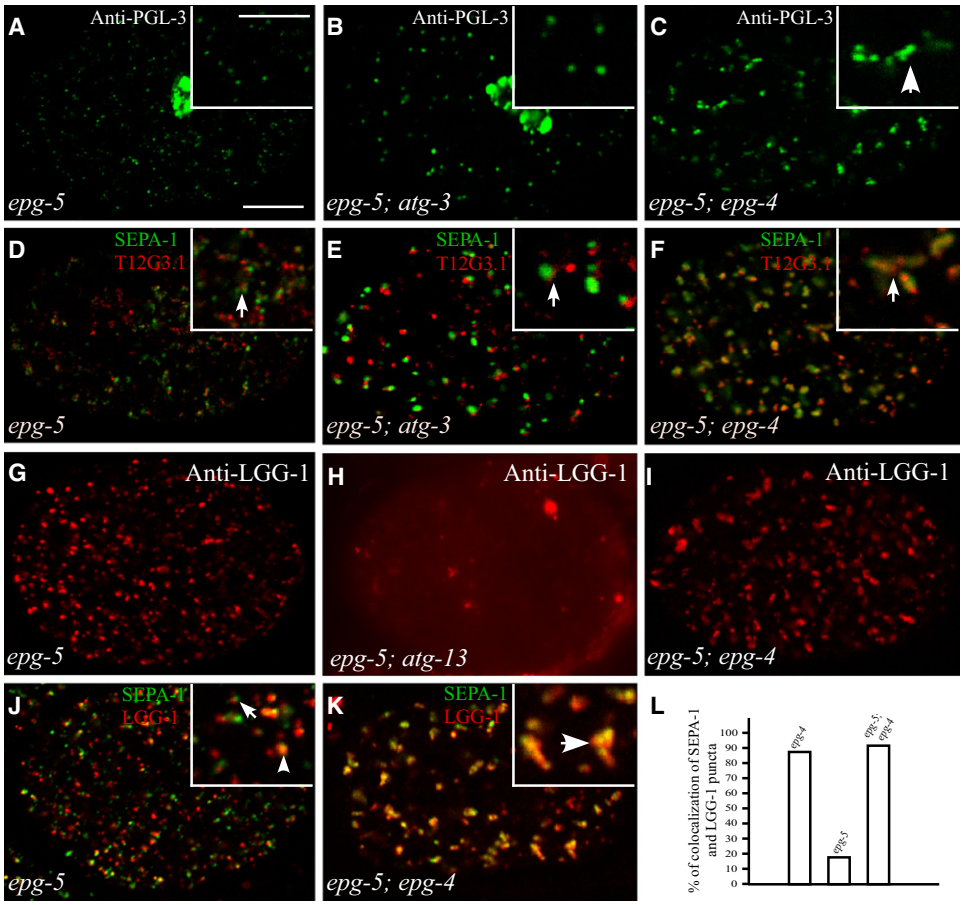

Figure 4. *epg-5* Functions at a Step Distinct from *atg-3* and *epg-4* in the Autophagy Pathway

(A and B) PGL granules are dispersed in the cytoplasm in *epg-5* (A) and *epg-5; atg-3* (B) mutant embryos.

(C) Formation of PGL granule clusters in *epg-5; epg-4* double mutants (arrow in the insert).

(D and E) SEPA-1 aggregates are in close proximity to, but do not colocalize with, T12G3.1 aggregates in *epg-5* (D) and *epg-5; atg-3* (E) mutants (arrows in the inserts).

(F) A large number of T12G3.1 aggregates colocalize with PGL granules in *epg-5; epg-4* mutants (arrow in the insert).

(G–I) Formation of LGG-1 puncta in *epg-5* (G), *epg-5; atg-13* (H), and *epg-5; epg-4* (I) mutant embryos.

(J) SEPA-1 aggregates are in close proximity to (arrow in the insert), or colocalize with (arrowhead in the insert), LGG-1 puncta in *epg-5* mutants.

(K) SEPA-1 aggregates colocalize with LGG-1 puncta in *epg-5; epg-4* mutants (arrow in the insert).

(L) Percentage of SEPA-1 aggregates that colocalize with LGG-1 puncta at the ~200 cell stage. *epg-5*: 18.1% (n = 701); *epg-5; epg-4*: 91.6% (n = 263). At the comma stage, 74.1% of SEPA-1 aggregates (n = 409) colocalized with LGG-1 puncta in *epg-5* mutants.

See also Table S1 and Figure S4.

or *atg-2* in *epg-5* mutants gave the characteristic distribution and organization of PGL granules and LGG-1 puncta seen in *epg-3*, *epg-4*, and *atg-2* single mutants (Figures 4C, 4F, 4I, 4K, and 4L; Table S1). Unlike *epg-3* and *epg-4* mutants, DFCP1::GFP punctate structures did not accumulate in *epg-5* mutant embryos (Figure S6). Thus, *epg-5* functions at a genetic step distinct from *epg-3*, *epg-4*, and other known autophagy genes in the autophagic degradation of protein aggregates.

Overexpression of *epg-4* and *epg-5*, but not *epg-3*, accelerates autophagic degradation of PGL granules in mutants with partial loss of function of *atg-3* and *atg-7*, but not in complete loss-of-function mutants of *lgg-1* and *atg-18* (Figure S3), indicating that EPG-4 and EPG-5 are rate-limiting factors in the autophagy pathway.

Loss of Function of *epg-2* Disrupts the Association of PGL Granules with LGG-1 Puncta

In *epg-2* mutants, PGL granules were spherical and dispersed in the cytoplasm and LGG-1 formed puncta (Figure 5A; Figure S5). Compared to wild-type embryos, the number of LGG-1 puncta exhibited no obvious difference in *epg-2* mutants. Unlike wild-type animals, in which the majority of SEPA-1 aggregates are colocalized with LGG-1 puncta, PGL granules localized separately from LGG-1 puncta in *epg-2* mutants (Figures 5C and 5F; Figure S5).

When *atg-2, epg-3*, *-4*, or *-5* were simultaneously depleted in *epg-2* mutants, the shape and organization of PGL granules were identical to those in *epg-2* single mutants (Figure 5B; Figure S5; Table S1). In the double mutants, LGG-1 still formed

large tubular and giant structures that were colocalized with T12G3.1 aggregates as in *atg-2*, *epg-3*, and *epg-4* single mutants (Figure 5D, Figure S5, and data not shown). PGL granules, however, were still separate from LGG-1 puncta in these double mutants (Figures 5E and 5F). PGL granules were also separate from LGG-1 puncta in *epg-2; epg-5* mutants (Figure S5; Table S1). Therefore, loss of function of *epg-2* specifically disrupts association of PGL granules with LGG-1 puncta.

EPG-2 Is Selectively Degraded by Autophagy

In autophagy mutants, EPG-2 aggregates accumulated dramatically and persisted in late-stage embryos and early larvae (Figures 5G and 5H; data not shown). Consistent with the result that EPG-2 is degraded by autophagy, EPG-2 aggregates colocalized with LGG-1 puncta in wild-type embryos (Figures 5J–5L). In wild-type and autophagy mutants, EPG-2 aggregates also colocalized with SEPA-1 aggregates (Figures 5M–5O and data not shown). EPG-2 directly interacted with LGG-1 and SEPA-1 (data not shown). These results suggest that EPG-2 is degraded by autophagy along with the PGL granule.

We next examined whether EPG-2 degradation requires PGL granule components. In *sepa-1* and *pgl-3* mutants, EPG-2 did not accumulate and colocalization of EPG-2 with LGG-1 puncta was unaffected (Figure 5I and data not shown). Thus, SEPA-1 and PGL-3 are dispensable for autophagic degradation of EPG-2, consistent with the idea that EPG-2 is an adaptor protein that brings PGL granules to LGG-1-containing autophagic structures.

Mammalian VMP1, EI24, and mEPG5 Are Required for Starvation-Induced Autophagy

We investigated whether *VMP1*, *EI24*, and *mEPG5*, encoding the mammalian EPG-3, -4, and -5 homologs, respectively, also play a role in autophagy. In mammalian cells, starvation-induced autophagy involves omegasome formation, autophagosome formation and maturation, fusion of autophagosomes with lysosomes, degradation of autophagosome cargo, and reformation of the lysosome from the autolysosome (Mizushima, 2007; Axe et al., 2008; Yu et al., 2010). The time for each step is highly reproducible in a given cell type. We examined the formation of LC3-positive structures in cells transfected with *VMP1*, *EI24*, or *mEPG5* siRNA, which effectively knocked down mRNA levels of the corresponding gene (Figure S7). In normal rat kidney (NRK) cells, in which the kinetics of the autophagic process is well characterized (Yu et al., 2010), autophagosomes are extensively induced after 2 hr starvation and autophagy activity starts to attenuate 2 hr later. Autophagosomes steadily decrease in number and largely disappear 10 hr after starvation (Yu et al., 2010). We found that 2 hr after starvation, LC3 punctate structures increased dramatically in *VMP1* knockdown cells, but not in *EI24* siRNA-treated cells (Figures 6A and 6B). Ten hours after starvation, LC3 punctate structures accumulated in both *VMP1* siRNA- and *EI24* siRNA-treated cells (Figures 6A and 6B). Because it was technically difficult to design siRNA for rat *mEPG5*, we studied *mEPG5* in HeLa cells, in which the peak of autophagosome formation is at 1 to 2 hr after starvation and autophagosomes largely disappear after 6 hr (Figure S7). LC3 punctate structures slightly increased in *mEPG5* siRNA cells 1 hr after starvation, but the increase was much more evident after 6 hr (Figures 6C and 6D). These results suggest that *VMP1* regulates an early step of the autophagy pathway, whereas *EI24* and *mEPG5* regulate a late step.

VMP1 Regulates the Duration of Omegasomes

Omegasomes are extensively induced after 1 hr of starvation and have an average duration of 4 min in NRK cells. Compared to cells transfected with nonspecific (NS) siRNA, the number of DFCP1-labeled omegasomes greatly increased in *VMP1* siRNA-treated cells (Figures 6E and 6F). Using time-lapse microscopy, we found that omegasomes persisted much longer in cells in which *VMP1* was knocked down (Figures 6G and 6H), which could explain the increased number of omegasomes in *VMP1* knockdown cells. Omegasomes colocalized with LC3-positive structures in *VMP1* knockdown cells (Figure 6I), suggesting that the increased number of LC3-positive structures in *VMP1* knockdown cells resulted from an increased number of omegasomes. In *VMP1* knockdown cells, LC3 puncta formed tubular and giant ring-shaped structures (Figures 6I and 6J). These results suggest that *VMP1* knockdown caused defective autophagosome formation. *VMP1* siRNA cells also exhibited defective fusion of LC3-positive structures with lysosomal-associated membrane protein 1 (LAMP1)-labeled lysosomes (Figure S7), which could be secondary effects of abnormal autophagosome formation.

We used TEM to investigate the defects in *VMP1* knockdown cells. Compared to NS siRNA-treated cells, there was a dramatic accumulation of isolation membranes in *VMP1* knockdown cells (Figure 6K). Consistent with the abnormal LC3-labeled structures, isolation membranes in *VMP1* knockdown cells were enlarged and formed ring-like or tubular structures (Figure 6K). Thus, knockdown of *VMP1* results in persistence of enlarged isolation membranes.

Knocking down *EI24* and *mEPG5* Causes Accumulation of Nondegradative Autolysosomes

To examine whether knockdown of *EI24* and *mEPG5* impairs autophagic degradation, we measured degradation of GFP-LC3. GFP-LC3 remains associated with the inner membrane of mature autophagosomes and, after its delivery to lysosomes, the GFP moiety is cleaved and remains relatively stable, whereas LC3 is rapidly degraded. The level of GFP, thus, has been widely used to measure autophagy activity (Mizushima et al., 2010). In NS siRNA-treated NRK cells, free GFP at high levels was detected 4 hr after starvation and the signal became weaker after 10 hr (Figure 7A). GFP-LC3 cleavage was almost completely blocked in *EI24* siRNA cells (Figure 7A). In HeLa cells, high levels of free GFP were detected after 2 hr starvation and GFP was completely degraded 6 hr after starvation. Knockdown of *mEPG5* blocked GFP degradation so that high levels of GFP persisted even after 10 hr starvation (Figure 7B). We repeatedly detected accumulation of GFP in nonstarved *mEPG5* knockdown cells, which could result from a defect in GFP degradation generated by constitutive basal autophagy. These results suggest that knockdown of *EI24* and *mEPG5* causes a defect in autophagic degradation.

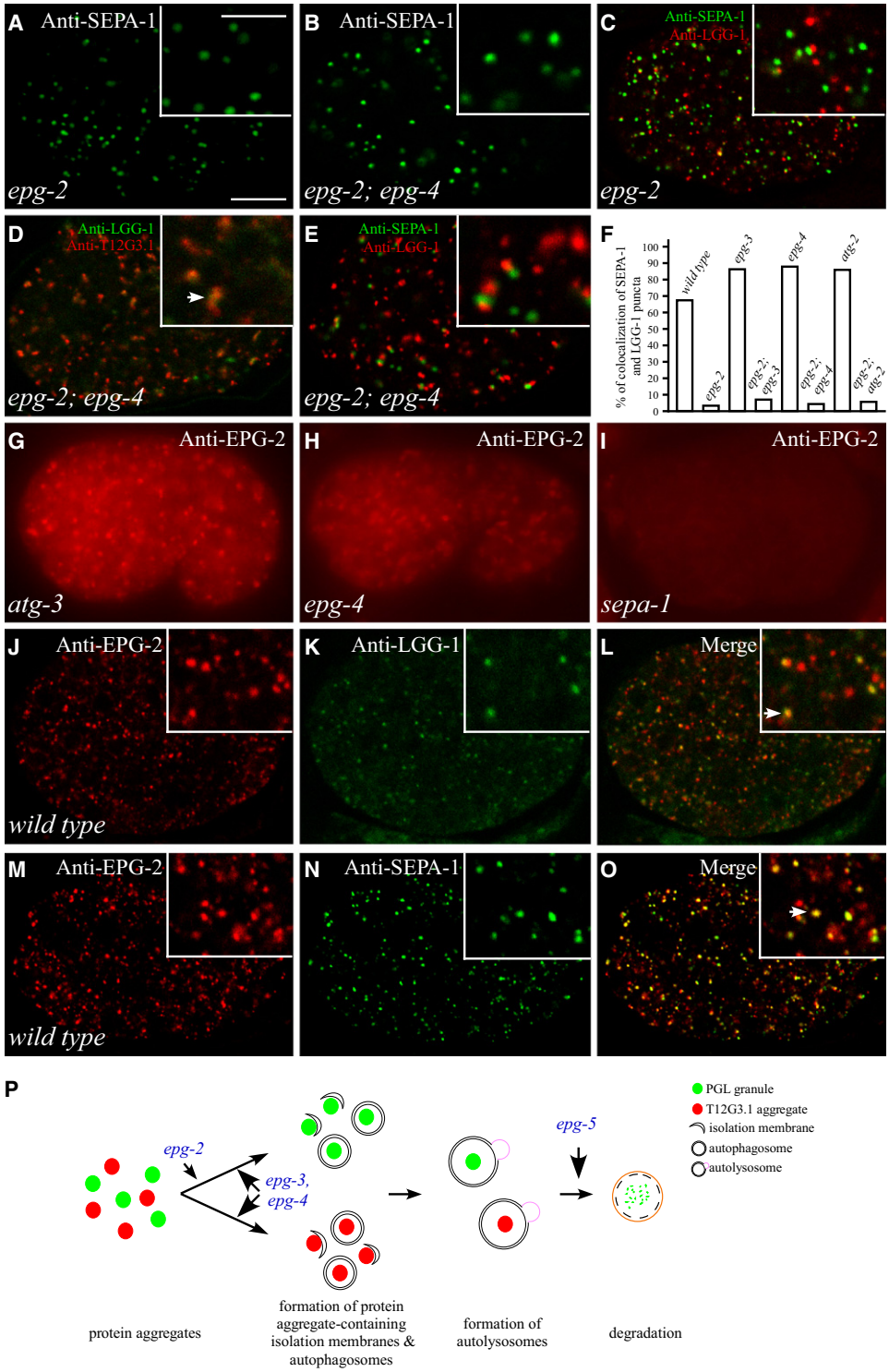

Figure 5. Loss of Function of *epg-2* Disrupts the Colocalization of PGL Granules with LGG-1 Puncta

(A and B) PGL granules are dispersed in the cytoplasm in *epg-2* (A) and *epg-2; epg-4* (B) mutant embryos.

(C) PGL granules (green) are separate from LGG-1 puncta (red) in *epg-2* mutants.

(D) T12G3.1 aggregates colocalize with enlarged LGG-1 puncta in *epg-2; epg-4* mutants (arrow in the insert).

(E) PGL granules do not colocalize with LGG-1 puncta in *epg-2; epg-4* mutants.

(F) Percentage of SEPA-1 aggregates that colocalize with LGG-1 puncta. *epg-2*: 3.1% (n = 256); *epg-2; epg-3*: 7.9% (n = 190); *epg-2; epg-4*: 4.1% (n = 98); *atg-2*: 86.3% (n = 154); *epg-2; atg-2*: 6.9% (n = 116).

Consistent with accumulation of LC3-positive structures at a late stage of autophagy, *EI24* and *mEPG5* knockdown caused no obvious defects in omegasome formation (data not shown). We investigated whether autophagosomes can fuse with lysosomes in *EI24* and *mEPG5* knockdown cells. In NRK or HeLa cells treated with NS siRNA, 8 hr (NRK) or 6 hr (HeLa) after starvation, the number of autolysosomes dramatically decreased due to attenuation of autophagy activity and reformation of lysosomes from autolysosomes (Yu et al., 2010). However, in cells treated with *EI24* and *mEPG5* siRNA at the same time points, LC3- and LAMP1-positive autolysosomes dramatically accumulated and these were also enlarged in *EI24* siRNA cells (Figures 7C and 7D). Inhibition of autolysosomal protein degradation by the lysosomal inhibitor leupeptin also resulted in enlarged, persistent autolysosomes (Yu et al., 2010). Leupeptin treatment did not further exacerbate the accumulation of autolysosomes in *mEPG5* knockdown cells (Figure S7). Knockdown of *EI24* and *mEPG5* appears to cause a defect in the degradation step of the autophagy pathway.

To demonstrate that autolysosome function is impaired, we stained *EI24* and *mEPG5* siRNA-transfected cells with DQ-BSA, a bovine serum albumin derivative conjugated to a self-quenched fluorophore. Lysosomal degradation of DQ-BSA releases fluorescent fragments, allowing the degradative capacity of autolysosomes to be monitored (Vázquez and Colombo, 2009). Compared to NS siRNA-treated cells, the fluorescent signal in autolysosomes was much lower in *EI24* and *mEPG5* siRNA-transfected cells (Figures 7E and 7F). Therefore, the proteolysis activity of autolysosomes was greatly impaired in *EI24* and *mEPG5* knockdown cells.

We performed TEM to examine the ultrastructure of autolysosomes in *EI24* and *mEPG5* knockdown cells. In NS siRNA-treated cells, autolysosomes were barely detected at 10 hr (NRK cell) or 6 hr (HeLa cell) after starvation (Figures 7G and 7H). However, autolysosomes accumulated dramatically in *EI24* and *mEPG5 siRNA*-treated cells (Figures 7G and 7H). Interestingly, the autolysosomes contained uniform electron-dense materials in *EI24* knockdown cells, whereas the autolysosomes in *mEPG5* knockdown cells contained heterogenous electron-dense and less dense contents. In summary, defects in autophagic degradation caused by reduced levels of EI24 and mEPG5 result in accumulation of autolysosomes in these cells.

DISCUSSION

EPG-2 Regulates the Association of PGL Granules with Autophagic Structures

EPG-2 is required for association of PGL granules with LGG-1 puncta. In *epg-2* mutants, PGL granule components form large numbers of aggregates that are separate from LGG-1 puncta. EPG-2 itself also forms aggregates that are degraded by autophagy and colocalize with PGL granules in wild-type and autophagy mutants. This is reminiscent of yeast Atg19, which mediates transport of aminopeptidase I (Ape1) from the cytoplasm to the vacuole in the Cvt pathway. Ape1 precursors (prApe1) form oligomers and then associate with the Atg19 receptor. Atg11 mediates delivery of the prApe1-Atg19 complex to the PAS and triggers formation of the Cvt vesicle. Atg19, but not Atg11, is degraded along with the prApe1 cargo (Xie and Klionsky, 2007). In *atg19* deletion cells, prApe1 forms a large complex but localizes separately from the PAS (Shintani et al., 2002). Thus, we propose that EPG-2 functions as a receptor linking PGL granules to the autophagic machinery. Direct interaction between the receptor (Atg19 and EPG-2) and Atg8/LGG-1 may ensure highly selective sorting of the cargo/receptor complex to autophagosomes. Unlike the Cvt pathway, in which Atg19 depends on prApe1 for aggregation and degradation (Shintani et al., 2002), formation and degradation of EPG-2 aggregates are independent of PGL granules. One possible explanation for this is that EPG-2 associates with and mediates the degradation of other unidentified protein aggregates during embryogenesis. It remains to be determined whether an Atg11-like protein transports the PGL-EPG-2 complex to specific autophagosome assembly sites, or whether autophagosomes form directly around the PGL-EPG-2 complex. Similar mechanisms using functional homologs of EPG-2 may be employed to degrade protein aggregates in other systems.

EPG-3/VMP1 Regulates an Early Step of Autophagosome Formation

EPG-3/VMP1 is involved in controlling the size and closure of isolation membranes and, thus, the formation of autophagosomes in *C. elegans* and mammalian cells (Figure 5P and Figure 7I). Loss of *epg-3/VMP1* function causes accumulation of enlarged LGG-1/LC3-labeled autophagic structures. PE-conjugated Atg8 has membrane tethering and hemifusion activities in vitro (Nakatogawa et al., 2007). These aberrant autophagic structures could result from homotypic fusion of precursors of autophagosomal membranes or isolation membranes. EM analysis shows accumulation of enlarged isolation membranes in *epg-3* mutants and *VMP1* knockdown mammalian cells.

VMP1 regulates autophagosome formation by controlling the duration of omegasomes. Omegasomes, which are in dynamic equilibrium with the ER, form a cradle for autophagosome formation (Axe et al., 2008; Hayashi-Nishino et al., 2009). Knockdown of *VMP1* causes accumulation of enlarged, persistent omegasomes. Omegasomes also accumulate and colocalize with LGG-1 puncta in *epg-3* mutant embryos. These enlarged, long-lasting omegasomes could cause the formation of enlarged, unclosed isolation membranes. Formation and expansion of omegasomes require the VPS34/Beclin 1 complex (Axe et al.,

(G and H) Large numbers of EPG-2 aggregates are found in comma stage *atg-3* (G) and *epg-4* (H) mutant embryos.
(I) EPG-2 is not ectopically expressed in *sepa-1* mutants.
(J–L) EPG-2 aggregates colocalize with LGG-1 puncta in a wild-type embryo (arrow in the insert).
(M–O) EPG-2 aggregates colocalize with SEPA-1 dots (arrow in the insert).
(P) Summary of the role of *epg-2*, *-3*, *-4*, and *-5* in the autophagy pathway. See Discussion for details.
See also Table S1 and Figure S5.

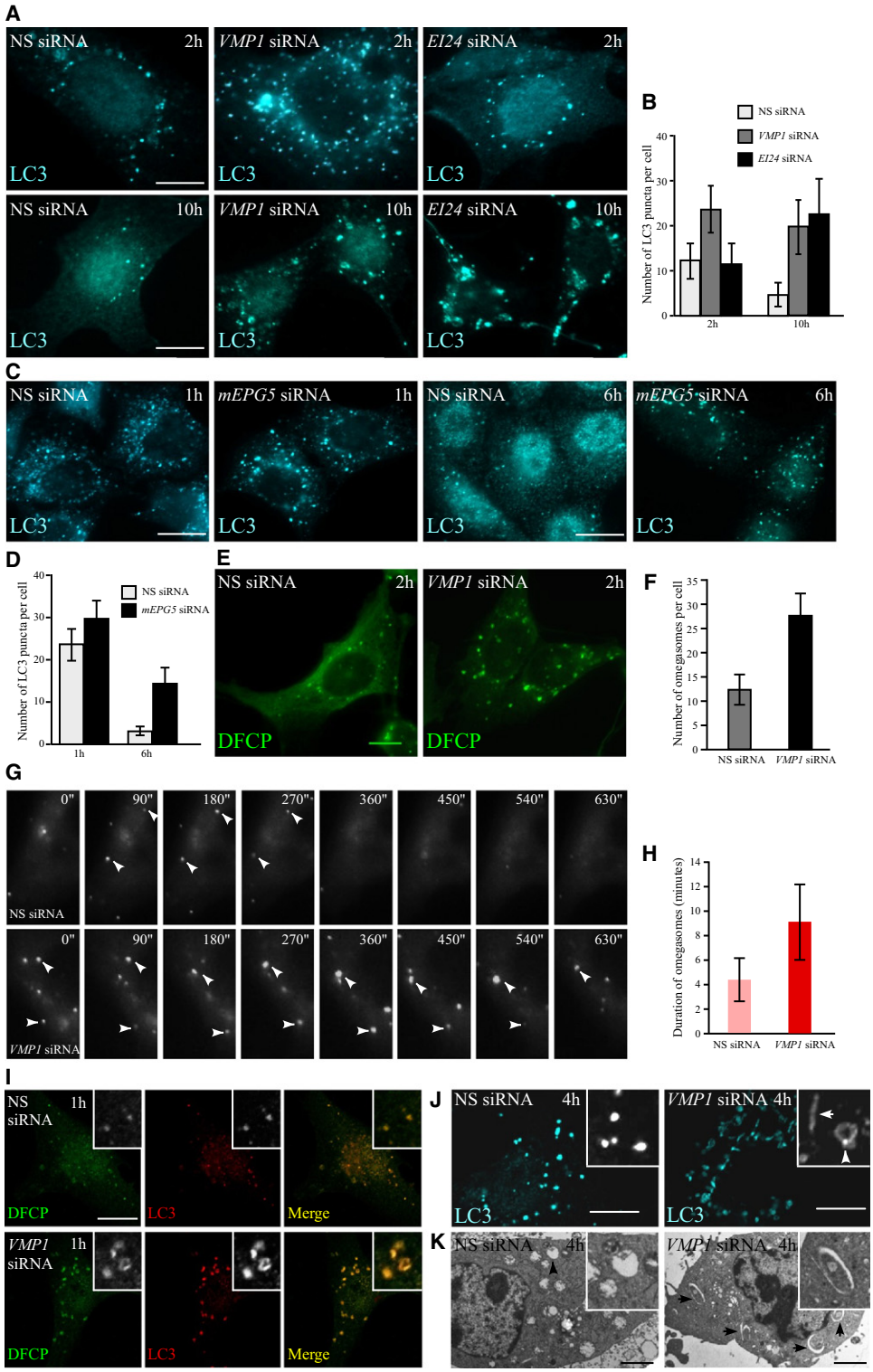

Figure 6. *VMP1* Regulates the Formation of Omegasomes and Autophagosomes

Scale bars (5 μm for fluorescence microscopy images and 2 μm for EM images) and time (hours) after starvation are indicated in each panel in Figure 6 and Figure 7. Experiments were performed in NRK cells for *VMP1* and *EI24* and HeLa cells for *mEPG5*.

(A) LC3-labeled autophagic structures, stained with anti-GFP antibody, in NRK-LC3-GFP cells treated with nonspecific (NS) siRNA or siRNA specific for *VMP1* or *EI24*.

(B) Average number of LC3-positive structures in NS, *VPM1*, and *EI24* siRNA-treated cells. One hundred cells were examined per time point. Data are represented as mean ± standard error of the mean (SEM).

2008). EPG-3/VMP1 may regulate the level and persistence of PI(3)P on omegasomes. The functional substitution of *epg-3* by human *VMP1* in degradation of PGL granules demonstrates that the role of *VMP1* in the autophagy pathway is conserved. Our data are in contrast to a previous study showing that *VMP1* knockdown blocks formation of LC3-labeled autophagic structures (Ropolo et al., 2007). The reason for this discrepancy is unknown. If *VMP1* is involved in multiple steps of the autophagy pathway, its loss of function might produce distinct defects in different cellular settings.

EPG-4/EI24 May Function at a Different Step of the Autophagy Pathway in *C. elegans* and Mammalian Cells

As in *epg-3* mutants, DFCP1-labeled omegasomes, enlarged LGG-1 puncta, and isolation membranes accumulate in *epg-4* mutant embryos, indicating that *epg-4* functions early in autophagosome formation (Figure 5P). The ER has been shown to be a source of autophagosomal membranes, and the ER and isolation membranes are interconnected (Hayashi-Nishino et al., 2009; Ylä-Anttila et al., 2009). In *epg-4* mutants, there is a high incidence of ribosome-free, cleft-like structures related to the RER, and multimembrane layers are found where isolation membranes normally form, indicating that the flow of membrane components and their reorganization into isolation membranes might be inhibited at this very early stage. EPG-4, an ER protein that contains six transmembrane domains, could be involved in transforming normal ER membranes into nascent isolation membranes.

Loss of *EI24* function has no effect on omegasome formation but results in accumulation of nondegradative autolysosomes in mammalian cells, indicating that *EI24* is involved late in the autophagy pathway (Figure 7I). The discrepancy between *epg-4* and *EI24* may be due to the relatively low knockdown efficiency of *EI24* siRNA. The defects in earlier autophagy steps (such as omegasome formation) are masked by the low siRNA efficiency and only the later cumulative defects become visible.

EPG-5/mEPG5 Regulates the Final Degradation Step of the Autophagy Pathway

Knockdown of *mEPG5* causes impaired autolysosomes to accumulate in mammalian cells. Although defective autolysosomes accumulate in both *mEPG5* and *EI24* knockdown cells, the underlying causes appear to be different. GFP-LC3 is largely uncleaved in *EI24* knockdown cells, whereas *mEPG5* siRNA cells show defective degradation of free GFP. Autolysosomes in *EI24* knockdown cells contain electron-dense materials, whereas in *mEPG5* knockdown cells they have heterogenous contents.

Our results are consistent with involvement of EPG-5 in the degradation step of the *C. elegans* autophagy pathway (Figure 5P). First, in contrast to *epg-3* and *epg-4* mutants, omegasomes do not accumulate in *epg-5* mutants. Second, SEPA-1 aggregates colocalize with LGG-1 puncta in *epg-5* mutants, suggesting that protein aggregates are enclosed by autophagic structures but fail to be degraded. Third, *epg-5* functions genetically downstream of the autophagy mutants we tested. Fourth, abnormal hybrids of late endosomes and lysosomes accumulate in the intestine cells in *epg-5* mutants (data not shown), indicating a role of *epg-5* in the lysosomal system.

In conclusion, this study demonstrates that *C. elegans* is a useful model system to identify and characterize higher eukaryote-specific autophagy genes, and our findings with this system provide a genetic framework for further study of basal and selective autophagic degradation of protein aggregates in mammalian cells.

EXPERIMENTAL PROCEDURES

Identification of *epg-2, -3, -4,* and *-5*

gfp::pgl-1, *sepa-1::gfp*, or *t12 g3.1::gfp* animals were used for EMS mutagenesis and F3 progeny were screened for accumulation of PGL-1, SEPA-1, or T12G3.1 aggregates in late-stage embryos. From ~30,000 genomes screened (~10,000 genomes for each reporter), 158 mutant alleles were isolated (28 from the *gfp::pgl-1* screen, 68 from the *sepa-1::gfp* screen, and 62 from the *t12 g3.1::gfp* screen). Details of the mapping and cloning of the mutants are in the Extended Experimental Procedures.

Reporter Construction

Reporters for *epg-3*, *-4*, *-5*, and *t12 g3.1* had *gfp* inserted at the C-terminal end and the *gfp::epg-2* reporter had *gfp* inserted at the N-terminal end. Expression of DFCP1::GFP was driven by the ubiquitously expressed *nfya-1* promoter. The DNA sequences used for constructing reporters are in the Extended Experimental Procedures.

Indirect Immunofluorescence

Permeabilization of embryos was performed by freeze-cracking methods. Freeze-cracked slides were fixed, blocked, and incubated with diluted antibody at room temperature for 2–4 hr, then washed three times and incubated with secondary antibody.

Cell Culture and Immunostaining

NRK and HeLa cells (from ATCC) were cultured in DMEM supplemented with 10% FBS (5% CO2), then transfected with 200 pmol siRNA (siRNA sequences are in Extended Experimental Procedures). Sixty hours after transfection, cells were starved, then collected at a specific time point for

(C) LC3-labeled autophagic structures in NS and *mEPG5* siRNA-treated cells.
(D) Average number of LC3-positive structures in NS and *mEPG5* knockdown cells. One hundred cells were counted per time point.
(E) Compared to control cells, omegasomes (labeled by DFCP1-GFP) accumulate in *VMP1* siRNA cells.
(F) Average number of omegasomes in NS and *VMP1* siRNA-treated cells 1 hr after starvation. One hundred cells were counted.
(G) Time-lapse images (seconds) of omegasomes (arrowed) in NS and *VMP1* siRNA cells. Cells were starved for 2 hr before analysis.
(H) Average duration time (minutes) of omegasomes in NS and *VMP1* siRNA-treated cells. Ten omegasomes were followed.
(I) Colocalization of omegasomes, detected by anti-GFP (DFCP1-GFP), and autophagosomes, stained by anti-LC3, in NS and *VMP1* siRNA cells. Inserts show magnified regions of interest.
(J) LC3 forms enlarged tubular structures (arrow) and giant complexes (arrowhead) in *VMP1* siRNA cells. (I and J) Confocal images.
(K) Accumulation of giant and tubular isolation membranes (arrows) in EM images of *VMP1* siRNA cells. In cells treated with NS siRNA at this time point, very few IMs are detected and many autolysosomes (arrowhead) are formed.
See also Figure S7.

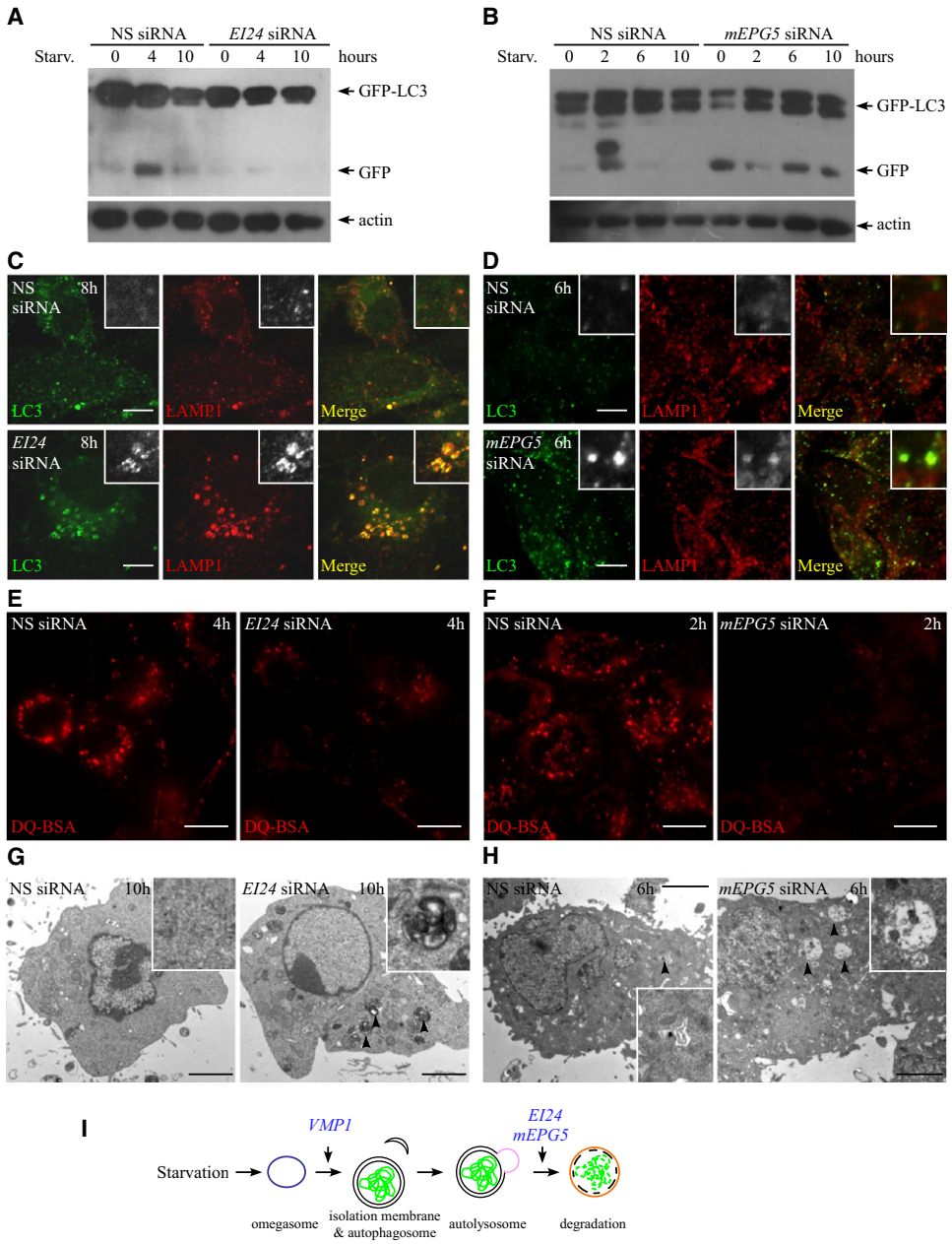

Figure 7. Knockdown of *EI24* and *mEPG5* Causes Accumulation of Nondegradative Autolysosomes

(A and B) Western blot showing a defect in degradation of GFP-LC3 in *EI24* and *mEPG5* siRNA-treated cells. siRNA-treated cells were starved for the indicated time (hours), harvested, and analyzed by western blot with anti-GFP antibody.

(C and D) Accumulation of LC3- and LAMP1-positive autolysosomes in *EI24* (C) and *mEPG5* (D) knockdown cells. (C and D) Confocal images.

(E and F) Autolysosomes stained with DQ-BSA in NS, *EI24*, and *mEPG5* siRNA-treated cells. Accumulation of fluorescent signal, generated from lysosomal proteolysis of DQ-BSA, is defective in *EI24* and *mEPG5* siRNA cells.

(G) EM images showing accumulation of autolysosomes (arrowheads) with electron-dense contents in *EI24* knockdown cells. Very few autolysosome-like structures are detected in NS siRNA cells at this time point.

(H) Accumulation of autolysosomes (arrowheads) in *mEPG5* siRNA-treated cells. The autolysosome contents are less electron dense.

(I) Model for *VMP1, EI24*, and *mEPG5* in the autophagy pathway.

See also Figure S7.

immunostaining or western blotting. To observe omegasomes, cells were transfected with siRNA. After 2 days, cells were again transfected with the corresponding siRNA and DFCP1-GFP. Sixteen hours after transfection, cells were starved for 2 hr before analysis. For the DQ-BSA assay, cells were transfected with siRNA. After 2 days, cells were starved for 4 hr and stained with DQ-BSA for 30 min.

SUPPLEMENTAL INFORMATION

Supplemental Information includes Extended Experimental Procedures, seven figures, and one table and can be found with this article online at doi:10.1016/j.cell.2010.04.034.

ACKNOWLEDGMENTS

We thank Dr Xiaodong Wang for comments on the manuscript; Edvard Burghardt, Mariann Sarody, Fan Wu, Tao Sun, and Hui Zhang for technical assistance; Dr. Shohei Mitani for *epg-5(tm3425)*; Dr. Gang Zhi and the NIBS antibody facility for preparing antibodies; and Dr. Isabel Hanson for editing services. This work was supported by the National High Technology Projects 863 (2008AA022306) (H.Z.) and Hungarian Scientific Research Funds OTKA K75843 (A.L.K.).

Received: November 12, 2009
Revised: February 27, 2010
Accepted: April 6, 2010
Published: June 10, 2010

REFERENCES

Axe, E.L., Walker, S.A., Manifava, M., Chandra, P., Roderick, H.L., Habermann, A., Griffiths, G., and Ktistakis, N.T. (2008). Autophagosome formation from membrane compartments enriched in phosphatidylinositol 3-phosphate and dynamically connected to the endoplasmic reticulum. J. Cell Biol. *182*, 685–701.

Dusetti, N.J., Jiang, Y., Vaccaro, M.I., Tomasini, R., Azizi Samir, A., Calvo, E.L., Ropolo, A., Fiedler, F., Mallo, G.V., Dagorn, J.C., and Iovanna, J.L. (2002). Cloning and expression of the rat vacuole membrane protein 1 (VMP1), a new gene activated in pancreas with acute pancreatitis, which promotes vacuole formation. Biochem. Biophys. Res. Commun. *290*, 641–649.

Eskelinen, E.L. (2005). Maturation of autophagic vacuoles in mammalian cells. Autophagy *1*, 1–10.

Fader, C.M., and Colombo, M.I. (2008). Autophagy and multivesicular bodies: two closely related partners. Cell Death Differ. *16*, 70–78.

Gu, Z., Flemington, C., Chittenden, T., and Zambetti, G.P. (2000). *ei24*, a p53 response gene involved in growth suppression and apoptosis. Mol. Cell. Biol. *20*, 233–241.

Hayashi-Nishino, M., Fujita, N., Noda, T., Yamaguchi, A., Yoshimori, T., and Yamamoto, A. (2009). A subdomain of the endoplasmic reticulum forms a cradle for autophagosome formation. Nat. Cell Biol. *11*, 1433–1437.

Kovács, A.L., and Zhang, H. (2010). Role of autophagy in *Caenorhabditis elegans*. FEBS Lett. *584*, 1335–1341.

Levine, B., and Kroemer, G. (2008). Autophagy in the pathogenesis of disease. Cell *132*, 27–42.

Longatti, A., and Tooze, S.A. (2009). Vesicular trafficking and autophagosome formation. Cell Death Differ. *16*, 956–965.

Meléndez, A., and Neufeld, T.P. (2008). The cell biology of autophagy in metazoans: a developing story. Development *135*, 2347–2360.

Mizushima, N. (2007). Autophagy: process and function. Genes Dev. *21*, 2861–2873.

Mizushima, N., Yoshimori, T., and Levine, B. (2010). Methods in mammalian autophagy research. Cell *140*, 313–326.

Nakatogawa, H., Ichimura, Y., and Ohsumi, Y. (2007). Atg8, a ubiquitin-like protein required for autophagosome formation, mediates membrane tethering and hemifusion. Cell *130*, 165–178.

Nakatogawa, H., Suzuki, K., Kamada, Y., and Ohsumi, Y. (2009). Dynamics and diversity in autophagy mechanisms: lessons from yeast. Nat. Rev. Mol. Cell Biol. *10*, 458–467.

Ropolo, A., Grasso, D., Pardo, R., Sacchetti, M.L., Archange, C., Lo Re, A., Seux, M., Nowak, J., Gonzalez, C.D., Iovanna, J.L., and Vaccaro, M.I. (2007). The pancreatitis-induced vacuole membrane protein 1 triggers autophagy in mammalian cells. J. Biol. Chem. *282*, 37124–37133.

Shintani, T., Huang, W.P., Stromhaug, P.E., and Klionsky, D.J. (2002). Mechanism of cargo selection in the cytoplasm to vacuole targeting pathway. Dev. Cell *3*, 825–837.

Sigmond, T., Feher, J., Baksa, A., Pasti, G., Palfia, Z., Takacs-Vellai, K., Kovacs, J., Vellai, T., and Kovacs, A.L. (2008). Qualitative and quantitative characterization of autophagy in *Caenorhabditis elegans* by electron microscopy. Methods Enzymol. *451*, 467–491.

Sjöblom, T., Jones, S., Wood, L.D., Parsons, D.W., Lin, J., Barber, T.D., Mandelker, D., Leary, R.J., Ptak, J., Silliman, N., et al. (2006). The consensus coding sequences of human breast and colorectal cancers. Science *314*, 268–274.

Suzuki, K., Kubota, Y., Sekito, T., and Ohsumi, Y. (2007). Hierarchy of Atg proteins in pre-autophagosomal structure organization. Genes Cells *12*, 209–218.

Vázquez, C.L., and Colombo, M.I. (2009). Assays to assess autophagy induction and fusion of autophagic vacuoles with a degradative compartment, using monodansylcadaverine (MDC) and DQ-BSA. Methods Enzymol. *452*, 85–95.

Xie, Z., and Klionsky, D.J. (2007). Autophagosome formation: core machinery and adaptations. Nat. Cell Biol. *9*, 1102–1109.

Ylä-Anttila, P., Vihinen, H., Jokitalo, E., and Eskelinen, E.L. (2009). 3D tomography reveals connections between the phagophore and endoplasmic reticulum. Autophagy *5*, 1180–1185.

Yu, L., McPhee, C.K., Zheng, L.X., Mardones, G.A., Rong, Y.G., Peng, J.Y., Mi, N., Zhao, Y., Liu, Z.H., Wan, F.Y., et al. (2010). Autophagy termination and lysosome reformation regulated by mTOR. Nature, in press. 10.1038/nature09076.

Zhang, Y.X., Yan, L.B., Zhou, Z., Yang, P.G., Tian, E., Zhang, K., Zhao, Y., Li, Z.P., Song, B., Han, J.H., et al. (2009). SEPA-1 mediates the specific recognition and degradation of P granule components by autophagy in *C. elegans*. Cell *136*, 308–321.